Volume 17
Number 26
14 July 2025
Pages 5311–5534

# Analytical Methods

rsc.li/methods


ISSN 1759-9679

ROYAL SOCIETY OF CHEMISTRY

**PAPER**
Alexander Gogos *et al.*
Alternative digestion strategy for Ti, Zr and Hf oxides: eliminating hydrofluoric acid

Indexed in Medline!

Analytical Methods

ROYAL SOCIETY OF CHEMISTRY

PAPER

View Article Online
View Journal | View Issue

Check for updates

Cite this: *Anal. Methods*, 2025, **17**, 5334

# Alternative digestion strategy for Ti, Zr and Hf oxides: eliminating hydrofluoric acid†

Lukas R. H. Gerken, [ab] Matthias Roesslein, [a] Inge K. Herrmann [abcd] and Alexander Gogos *[ab]

Group IV metal oxides have a broad impact on the environment and human health due to their diverse applications in industry, consumer products and biomedicine. However, their chemical inertness poses significant challenges for accurate quantification in biological matrices, which is essential for assessing biodistribution, toxicity, and regulatory compliance. Traditional digestion methods often rely on hydrofluoric acid (HF), a hazardous reagent requiring specialized handling and infrastructure. Here, we present an alternative, HF-free microwave assisted digestion protocol for group IV metal oxides in biological contexts, utilizing sulfuric acid/water/hydrogen peroxide mixtures to achieve complete solubilization across nano-to microscale particles. The method's efficacy was evaluated on various commercially available $TiO_2$, $ZrO_2$, and $HfO_2$ powders. Optimization of digestion parameters, including acid-to-peroxide ratios, temperature, and reaction time, led to recoveries exceeding 90% for all tested materials. Notably, higher temperatures and extended digestion times were required for larger particles and higher atomic number oxides, reflecting the increased metal–oxygen bond dissociation energies. The method's applicability was further demonstrated through successful quantification of spiked nanoparticles in human cancer cells and bovine liver tissue, with detection limits down to ~1 ppb and achieving recoveries within 80–100%, maintaining sample stability over four weeks. Comparative analysis with HF-based digestion revealed comparable sensitivity and detection limits using inductively coupled plasma optical emission spectrometry (ICP-OES), with the HF-free method offering a safer and more accessible alternative for routine laboratory analysis. This validated protocol facilitates accurate quantification of group IV metal oxides in complex biological matrices, supporting preclinical and clinical studies while mitigating the risks associated with HF usage.

Received 30th April 2025
Accepted 2nd June 2025

DOI: 10.1039/d5ay00731c

rsc.li/methods

Open Access Article. Published on 03 June 2025. Downloaded on 5/18/2026 3:39:33 AM.
This article is licensed under a Creative Commons Attribution 3.0 Unported Licence.

## Introduction

Group IV metal (Ti, Zr, Hf)-containing materials are utilized in various biomedical and consumer-good applications, including cancer therapy, dental and orthopaedic implants, pigments, catalysts and coatings.[1–10] This is primarily due to their biocompatibility and desirable mechanical, electrical or (physico)chemical properties. For instance, Ti and Ti alloys (*e.g.*, $Ti_6Al_4V$) are employed in long-lasting, load-bearing medical implants due to their elastic modulus, which closely resembles that of bone, and their naturally occurring oxide surface. Zirconium oxide ($ZrO_2$) serves as a dental ceramic implant material owing to its white color, high biocompatibility, low thermal conductivity, toughness, and low bacterial attraction.[11,12] Although these materials are typically used as bulk implants, it is now well documented (*e.g.*, refs. 13–15) that wear particles are released and accumulate in surrounding tissues, highlighting an increasing need for biodistribution analysis and a better understanding of their material fate. In nanoparticulate form, group IV metal oxides and metal–organic frameworks (MOFs) show promise as anticancer agents due to their photocatalytic, radiocatalytic, or X-ray absorption properties.[16] For example, nano-$TiO_2$ exhibits significant photocatalytic activity and can be used in photodynamic cancer therapies.[17] Similarly, Zr- and Hf-carrying nanomaterials demonstrate promising X-ray radiation-based anticancer effects.[18–20] Some of these materials are under clinical investigation,[21,22] or have received regulatory approval for pharmaceutical applications (*e.g.*, by the FDA).[23] All in all, the various

[a]*Laboratory for Nanomaterials in Health, Department of Materials Meet Life, Swiss Federal Laboratories for Materials Science and Technology (Empa), Lerchenfeldstrasse 5, St. Gallen, 9014, Switzerland. E-mail: alexander.gogos@empa.ch; Tel: +41(0)58 765 78 05*

[b]*Nanoparticle Systems Engineering Laboratory, Institute of Process Engineering, Department of Mechanical and Process Engineering, ETH Zurich, Sonneggstrasse 3, Zurich, 8092, Switzerland*

[c]*Ingenuity Lab, University Hospital Balgrist, Forchstrasse 340, Zurich, 8008, Switzerland*

[d]*Faculty of Medicine, University of Zurich, Rämistrasse 71, Zurich, 8006, Switzerland*

† Electronic supplementary information (ESI) available. See DOI: https://doi.org/10.1039/d5ay00731c



This journal is © The Royal Society of Chemistry 2025

Open Access Article. Published on 03 June 2025. Downloaded on 5/18/2026 3:39:33 AM. This article is licensed under a Creative Commons Attribution 3.0 Unported Licence.

use cases in research suggest group IV metals will have increasing impact in the future.

For clinical translation, it is imperative to gain insights into the stability, biotransformation, uptake behavior, and biodistribution of these materials. Additionally, metal analysis in tissues surrounding medical implants is necessary to understand tissue reactions and the release of metal ions or wear particles.[24] Therefore, there is a growing need to quantify these materials in different complex matrices such as culture media, blood, cells and tissues. This is also reflected in demands from regulatory authorities such as the FDA,[25] that emphasize biodistribution and uptake studies, especially for non-biodegradable materials.

However, non-validated methods are often used in the biomedical community (*e.g.* aqua regia for Hf[26,27]) or actual concentrations are not even determined.[28] Validated methods for determining group IV oxides are often either hazardous or labour-intensive and therefore often not performed or implementable in standard labs. Due to passivation, $TiO_2$ as well as $ZrO_2$ and $HfO_2$ do not dissolve in cold mineral acids with the exception of hydrofluoric acid (HF).[29] Consequently, most common digestion protocols involve HF in combination with other acids, such as nitric acid ($HNO_3$) to break down the oxides and stabilize the analyte ions as fluoride complexes. The use of HF necessitates stringent safety measures and trained personnel as it poses significant health risks upon skin contact and requires immediate medical action upon an incident. Due to these risks and associated costs, alternative digestion methods have been explored, particularly for $TiO_2$, one of the most studied nanoscale inorganic materials. Most commonly, fusion reactions have been shown to break down $TiO_2$. For example, $SiO_2$ has been determined in a $TiO_2$ matrix using alkali fusion with KOH and boric acid, followed by dissolution in dilute HCl.[30] Many other methods rely on fusion with sulfates. For instance, $TiO_2$ has been determined in sunscreens using a three-step sequential microwave digestion in a 1 : 1 mixture of $HNO_3$/HCl followed by fusion in a crucible with $KHSO_4$ and subsequent dissolution in $H_2SO_4$.[31] Furthermore, ammonium persulfate fusion in a crucible followed by soaking in 2% $HNO_3$ and subsequent hot plate boiling was employed to determine $TiO_2$ in water and wastewater.[32] Titanium dioxide has also been analyzed in chewing gum by heating a sulfuric acid and catalyst mixture to 400 °C for 2 hours in a Kjeldahl unit, followed by dilution to 10% $H_2SO_4$ for measurement.[33]

The success of such sulfate-based alternative methods is not surprising, since $TiO_2$ in concentrated $H_2SO_4$ is known to form Ti(IV)sulfate ($Ti(SO_4)_2$), which is colorless and dissociates in water. Titanium(IV) also forms different complexes in sulfuric solutions, *e.g.* $[Ti(OH)_2]^{2+}$, $[Ti(OH)_3]^{+}$, $[Ti(OH)_2(HSO_4)]_{aq}$ and $[Ti(OH_3(HSO_4)]_{aq}$.[29] Similarly, Zr and Hf form sulfates in sulfuric solutions, including $(Zr(SO_4)_2 \cdot 4H_2O$, $Hf(SO_4)_2 \cdot 4H_2O$, $Zr(OH)_2SO_4$ and $Hf(OH)_2SO_4 \cdot H_2O$.[34] Therefore, generating sulfate complexes presents a promising route for solubilizing group IV oxides without using HF. For instance, Ma *et al.* used $H_2SO_4$ to extract Zr and Hf with recoveries of 89.1 and 81.2%, respectively, from a zirconosilicate.[35] Furthermore, Watkins *et al.* demonstrated in 2018 that using $H_2SO_4$/water mixtures and heating to 110 °C for 8 hours effectively digested nano-$TiO_2$ in various matrices including water, fish tissue, periphyton and sediment.[36] Based on these results, we evaluated this approach in a previous study, where we achieved recoveries between 96 and 107% for Ti, Ti/Zr and Hf-containing metal–organic frameworks.[37]

Encouraged by these results, we further evaluated, developed and validated this HF-free digestion method also for the oxides, which were expected to be more difficult to solubilize. In this study, we investigated and validated the use of a sulfuric acid-hydrogen peroxide-based microwave digestion to quantitatively dissolve group IV oxides in nano- and microparticulate form as a cost effective, quick and readily available alternative to HF and fusion-based methods. We assessed the digestion performance of $TiO_2$, $ZrO_2$ and $HfO_2$ powders with different, clinically and industrially relevant primary particle sizes from several nm up to microns. After optimizing digestion parameters such as temperature, digestion time and acid/peroxide ratios with the parent powders we finally optimized and demonstrated the applicability of the validated method to quantify these materials in cancer cells and tissues.

## Materials and methods

### Particles, chemicals and reagents

For our experiments, we chose commercially available materials where applicable to allow for accessibility for future comparative experiments. Most of the metal oxide powders were available from Sigma Aldrich. The respective product and CAS numbers can be found in Table S1 in the ESI.†

All reagents were of analytical grade unless stated otherwise. Concentrated $HNO_3$ (69%), $H_2SO_4$ (97%), $H_2O_2$ (30%) as well as HF (40%) were obtained from Sigma Aldrich. Ultrapure water (18.2 MΩ) was obtained through an ELGA Chorus purification device. NIST-traceable certified reference materials (CRM) for instrument calibration were obtained from inorganic ventures.

### Digestion procedures

In total, we evaluated five different digestion procedures and compared them to a combination of $HNO_3$, $H_2O_2$ and HF as the "gold standard" method of reference for the selected materials.

**Method I**: 1.5 mL $HNO_3$ (65%) and 1 mL $H_2O_2$ (30%) were added to the weighted particle powder in a quartz glass tube. The samples were digested in 10 mL quartz tubes closed by a PTFE cap with pressure-exchange opening in a pressurized microwave (TurboWAVE, MLS GmbH) at 120 bar pressure and 200 °C for 10 min, after an initial ramping phase from room temperature to 200 °C of 12 min.

**Method II**: 1 mL ultrapure $H_2O$, 1.5 mL $H_2SO_4$ (97%) and 1 mL $H_2O_2$ (30%) were added to the weighted particle powder in the quartz digestion tubes. The samples were digested in the pressurized microwave at 120 bar pressure and 200 °C for 10 min, after an initial ramping phase from room temperature to 200 °C of 12 min.

**Method III**: 1 mL ultrapure $H_2O$, 1.5 mL $H_2SO_4$ and 1 mL $H_2O_2$ were added to the weighted particle powder in the quartz

Open Access Article. Published on 03 June 2025. Downloaded on 5/18/2026 3:39:33 AM. This article is licensed under a Creative Commons Attribution 3.0 Unported Licence.

digestion tubes. The samples were digested in the pressurized microwave at 120 bar pressure and 250 °C for 30 min, after an initial ramping phase from room temperature to 250 °C of 12 min.

**Method IV**: The particle powders were digested in 1.5 mL $H_2SO_4$ and 1 mL $H_2O_2$ using the otherwise same procedure as in method III. Since the digestion matrix is an acid piranha solution requiring special precautions,[33] we first placed all quartz digestion tubes containing the samples into a cold water bath, then added $H_2SO_4$ and finally, slowly, $H_2O_2$. Both reagents did not immediately mix and react, and a short agitation using a vortex was necessary. After careful agitation, the samples were immediately placed back into the cold water bath, as in all cases an exothermic reaction could be observed. The reactions observed were never violent, *i.e.* we did not observe heating to $\gg$100 °C or very extensive foaming/effervescence or even deflagration.

**HF reference method**: For comparison, the HF-digestion was performed by adding 2 mL $HNO_3$, 1 mL $H_2O_2$ and lastly 0.3 mL HF (40%) in a protected HF-facility to pre-weighted particle powders. Samples were digested in Teflon tubes at 250 °C and 120 bar for 10 min after a temperature ramping time of 15 min using an ultraCLAVE (MLS GmbH) microwave.

After any digestion method, the samples were transferred to conical 50 mL polypropylene test tubes and filled to the mark with ultrapure water and measured without further dilution (unless stated otherwise) using an inductively-coupled plasma optical emission spectrometer (ICP-OES). All measured concentrations and recovery calculations can be found in the ESI, in Tables S3–S7.†

### Instrumentation

For all measurements, an Agilent 5110 ICP-OES was used. Sample introduction was performed *via* an SPS4 autosampler connected to a glass concentric nebulizer followed by a glass cyclonic double pass spray chamber. Operating parameters of the instrument are summarized in Table S2 (ESI).† Calibration curves for all elements of interest were made from single element standards (CRMs) obtained from inorganic ventures (Suisse TP product numbers: CGTI1 (Ti), CGZR1 (Zr) and CGHF1 (Hf)) and were prepared in an acid solution matched exactly to the respective samples. Specifically, the calibration solution matrix for the HF-free digestion solutions consisted of 2.91% v/v $H_2SO_4$, corresponding to 1.5 mL $H_2SO_4$ (97%) per 50 mL total volume, whereas that for the HF digestion solutions contained 2% v/v $HNO_3$. Calibrations were additionally verified by measuring a certified multi-element standard (CCS-5, Inorganic Ventures). Recoveries for all elements were usually >96% in this case. Data were initially evaluated using the software ICP-expert (v7.4.1.10449, Agilent Technologies) to calculate mass concentrations from intensities before they were exported for further analysis.

### Method development and spiking experiments

Initial method development was carried out with pure powders. To distribute a defined particle mass to the digestion tubes, first a 1 mg $mL^{-1}$ aqueous dispersion of each powder was prepared by accurately weighing the powder into a small 2 mL glass vial (VWR). After weighing, ultrapure water was added so that the final mass concentration reached 1 mg $mL^{-1}$. From this dispersion, defined aliquots were then distributed to the digestion tubes after reaching a homogenous sample dispersion using vortex agitation and ultrasonication and it was proceeded as described above. Similarly, for cell spiking experiments, 10 μL of the homogenous nanoparticle dispersion was added to 100.000 HT1080 cancer cells, corresponding to <0.1 ng metal mass per cell or <10 wt%. Cells were previously taken from a routinely cultured cell flask. Cells were cultivated in minimum essential medium eagle (MEM, Sigma-Aldrich) supplemented with 10% fetal calf serum, 1% L-glutamine, 1% penicillin–streptomycin, 1% nonessential amino acids, and 1 mm sodium pyruvate. To detach cells from a flask, HT1080 cells (ATCC CCL121TM) were trypsinized and counted using a hemocytometer. One million cells per mL solution were recovered and 100.000 cells were added to each quartz digestion tube before nanomaterial dispersions were spiked. Standard culturing practices that were used are described elsewhere.[3]

For tissue spiking, the CRM BCR 185R (bovine liver, powder) was weighed in approx. 20 mg aliquots to the quartz tubes and mixed with 200 μL of the homogenous particle dispersion, corresponding to <1 wt% nanomaterial uptake; clinically relevant cell or tissue uptake scenarios are considered to be below 10 wt% of metal uptake.[39] For instance, for intratumoral nanoparticle injections of NBTXR3 ($HfO_2$) a total oxide mass of 1.8 wt% should be injected, corresponding to 1.5 wt% of Hf.[40]

### Method validation

The accuracy of the method was determined from best estimates for a true value obtained from own spiking experiments, as no certified reference materials for group IV oxides in biological material were available. Specifically, the accuracy was evaluated by relating the measured metal mass, $m_{\text{meas.}}$, to an expected metal mass (*i.e.*, best estimate for the true value), $m_{\text{exp.}}$, as follows:

$$\text{Recovery } (\%) = \frac{m_{\text{meas.}}}{m_{\text{exp.}}} = \frac{c_{\text{meas.}} \times V_s}{(m_{\text{MO}} \times (1 - \text{SR}) \times f_M) \times (V_s)^{-1}} \quad (1)$$

$m_{\text{meas.}}$ = metal mass in the sample. $m_{\text{exp.}}$ = expected metal mass. $c_{\text{meas.}}$ = metal concentration in the sample. $V_s$ = sample volume. $m_{\text{MO}}$ = mass of the metal oxide powder. SR = water and organic surface residue mass fraction determined from thermogravimetric analysis. $f_M$ = metal mass fraction of the respective metal oxide with 0.848 (M = Hf), 0.740 (M = Zr) and 0.599 (M = Ti).

Furthermore, we determined the method precision according to the following condition:[41]

$$\Delta x(\%) = \frac{|x_1 - x_2|}{\bar{x}} \times 100 \leq \sqrt{2} \times 2 \times s_{v,\text{rel}} \quad (2)$$

$\Delta x(\%)$ = relative difference of measured values to the mean. $x_{1,2}$ = measured values. $\bar{x}$ = average of measured values. $\sqrt{2}$ = root of replicate number ($n = 2$). $s_{v,\text{rel}}$ = relative standard deviation – set to a limit of 2%.

 This journal is © The Royal Society of Chemistry 2025

Open Access Article. Published on 03 June 2025. Downloaded on 5/18/2026 3:39:33 AM. This article is licensed under a Creative Commons Attribution 3.0 Unported Licence.

In our case for method II–IV, this condition was fulfilled with $\overline{\Delta x} = 2.8\% \leq \sqrt{2} \times 2 \times 2\% = 5.65$, hence digestions were performed in duplicates. All experimentally determined as well as calculated values for each experiment can be found in Tables S3–S7 in the ESI.† Furthermore, sample stability was determined by measuring the same samples after a specific time with a fresh calibration.

### Thermogravimetric analysis

Water and organic surface content was assessed using thermogravimetric analysis (TGA) and was performed with a NETZSCH TG 209 F1 instrument (NETZSCH-Gerätebau GmbH, Selb, Germany) and heating of the weighted sample at room temperature to 700 °C, with a heating rate of 10 °C $min^{-1}$ under nitrogen flow. The surface residue mass fraction (SR) was quantified from the weight loss at 700 °C.

### X-ray diffraction

X-ray powder diffraction was performed on a PANalytical X'Pert Powder Diffractometer (Malvern Panalytical, UK) equipped with a copper X-ray source. Particle powders were placed on a low background sample holder and diffraction patterns were recorded from the rotating powder sample. Rietveld refinement for phase and grain size analysis was performed using Profex[42] (Version 4.3.5).

## Results and discussion

### Particle characterization and reference digestion

Prior to determining element/oxide recoveries, all nano- and microparticles were characterized to confirm or estimate the theoretical element composition, their sizes and potential organic surface residues. X-ray powder diffraction (XRD) patterns indicated that all particles were crystalline (ESI, Fig. S1†). Based on XRD Rietveld refinement calculations, nanoparticles had grain sizes around 9–25 nm, while microparticles ranged from 26 to 107 nm (Table 1). Phase analysis identified typical metal oxide specific phases. While most particles were present in a major single phase, nano $HfO_2$ and nano $TiO_2$ displayed multiple phases. The analysis also confirmed the respective phases for micro anatase $TiO_2$ and micro rutile $TiO_2$ as specified by the distributor. Transmission electron microscopy (TEM) corroborated the nanometer-scale sizes, ranging from 6 to 34 nm ($d_{TEM}$), suggesting a single crystalline domain per nanoparticle. Hafnium dioxide was the smallest nanoparticle, followed by $TiO_2$ and $ZrO_2$. The sizes of all microparticles were estimated using scanning electron microscopy (SEM) images and were well above the XRD grain sizes, implying multiple crystalline domains per microparticle. $HfO_2$, $ZrO_2$ and anatase $TiO_2$ exhibited average particle sizes between 150 and 280 nm ($d_{SEM}$). Rutile $TiO_2$ was the biggest microparticle with an average size of 860 nm. All nano- and microparticles were spherical to elliptical in shape (ESI, Fig. S2†). Given that nanomaterials possess a higher surface area than micromaterials, they are more prone to adsorbing moisture or other volatile organic substances on their surface. To estimate the amount of such surface adsorbed volatile substances, and with this also the inorganic metal oxide particle weight, thermogravimetric analysis (TGA) was performed (ESI, Fig. S3†). Microparticles exhibited minimal mass loss (<0.2%) after heating to 700 °C, as expected. In contrast, nanoparticles showed notable volatile organic surface residues ranging from 0.7 to 2.6 wt%. Interestingly, the amount of surface residues was highest for the smallest nanoparticle and decreased with particle size, which is in line with the higher surface area of smaller nanoparticles. These surface residues were accounted for in calculating the metal oxide purity correction factor (1-SR, eqn (1)). Subsequently, metal recovery investigations were performed using ICP-OES with the state-of-the-art HF digestion method as a reference for developing an HF-free digestion method. As expected, the HF method efficiently solubilized the selected materials, yielding recoveries between 93 and 106%. For nano $HfO_2$, we noted an increased recovery of slightly over 100%, which might be attributed to minor contaminations. However, all recoveries were compliant to FDA criteria; according to the FDA, an acceptable recovery range for an element in drug testing is between 80% and 120% of the declared content to ensure method accuracy and reliability.[43]

Furthermore, we noted impurities of Zr in Hf oxide and *vice versa*. The metal impurity of Zr in $HfO_2$ materials was quantified to be <0.2% (micro) and <1.2% (nano) (Zr/Hf). The impurity of Hf in $ZrO_2$ materials, however, was around ~2% (Hf/Zr) (ESI,

Table 1 Material properties (crystal size and phase, particle size and surface residues) of the particles used in this study and calculated oxide recovery rate (eqn (1), ESI, Table S3) after HF digestion. Corresponding XRD spectra, EM images and size distributions can be found in the (ESI)

| Material | | Grain size value ± ESD (nm) | Main phase | dTEM/SEM average ± SD (nm) | Surface residue, SR mass loss (weight %) | Recovery HF reference method ($n = 2$) (%) |
|---|---|---|---|---|---|---|
| $HfO_2$ | Micro | 68.1 ± 0.4 | Monoclinic (>99%)[46] | 150.4 ± 66 | ~0.1 | 95.4 ± 3.7 |
| $ZrO_2$ | | 26.4 ± 0.2 | Monoclinic (>98%)[47] | 276.4 ± 103 | ~0.2 | 96.4 ± 1.2 |
| $TiO_2$ | | 39.1 ± 0.2 | Anatase (>99%)[48] | 218.5 ± 76 | ~0.1 | 97.1 ± 0.4 |
| $TiO_2$ | | 127.1 ± 1.2 | Rutile (>96%)[49] | 859 ± 370 | ~0 | 96.8 ± 1.2 |
| $HfO_2$ | Nano | 8.9 ± 1.1 | Monoclinic (>83%)[46] | 5.8 ± 1.5 | ~2.6 | 105.5 ± 2.0 |
| | | 12.4 ± 3.5 | Orthorhombic (>15%)[50] | | | |
| $ZrO_2$ | | 25.4 ± 0.2 | Monoclinic (>99%)[47] | 31 ± 7.5 | ~0.7 | 93.5 ± 1.0 |
| $TiO_2$ | | 14.8 ± 0.1 | Anatase (>93%)[48] | 16.5 ± 6.3 | ~2.0 | 95.5 ± 0.4 |
| | | 18.7 ± 0.8 | Rutile (>6%)[49] | | | |

Open Access Article. Published on 03 June 2025. Downloaded on 5/18/2026 3:39:33 AM. This article is licensed under a Creative Commons Attribution 3.0 Unported Licence.

Table S3†). These impurities were excluded from the recovery calculations. Zirconium (Zr) and hafnium (Hf) commonly coexist in natural minerals[44] making them mutual impurities in each other's materials. Major Zr sources include Zircon ($ZrSiO_4$) and baddeleyite (natural form of $ZrO_2$) in which Zr and Hf coexist.[45] Zircon is the primary source of all Hf and contains up to 1.2 wt% Hf.[45] Since they are chemically nearly identical, separating these elements remains challenging[45] explaining the observed presence of impurities.

### Digestion method optimization using pure powders

Initially, materials were digested using a commonly employed HF-free method comprising only $HNO_3$ and $H_2O_2$ (method I, Fig. 1) and compared to the reference HF digestion. This approach resulted in unacceptably low recoveries (<30%) for all microparticles. Similarly, nano $ZrO_2$ exhibited a low recovery (~20%) with this simple nitric acid/peroxide digestion. Consequently, this method also did not fulfill our precision criterion (see eqn (2) and ESI Table S4†), which is expected for such low recoveries. Interestingly, the recovery for nano $TiO_2$ and nano $HfO_2$ was found to be around 80%. Compared to microparticles, nanoparticles have a higher accessible surface area increasing digestion probability. Additionally, sufficiently small and colloidally stable nanoparticles are likely to achieve good atomization efficiency in the ICP plasma without complete digestion. For instance, slurries with particles below ~5 μm often achieve good atomization in the plasma and recoveries comparable to digested solutions.[51,52] Such size effects could explain the high recoveries of $TiO_2$ and $HfO_2$ nanoparticles, which are smaller than nano $ZrO_2$ and all microparticles, using the simple nitric acid route.

Subsequently, nitric acid was replaced with an aqueous 60% $H_2SO_4$ mixture (digestion method II). This change significantly improved nanoparticle recoveries to acceptable levels (90–100%). Consequently, also the precision was improved considerably to ~1.6 $\Delta x$(%). Microparticle recoveries also improved, following an atomic number ($Z$) dependent trend. Notably, micro Anatase $TiO_2$ was recovered at nearly 100% while the rutile form achieved around 70%. Given that rutile $TiO_2$ had a much larger particle size, the differing recoveries between $TiO_2$ phases likely resulted from size and grain size differences in the micropowders.

Compared to $TiO_2$, micro $ZrO_2$ and micro $HfO_2$ had lower recoveries (~50% and ~20%, respectively). This behavior suggests an atomic number-dependent recovery rate trend, consistent with the Z-dependent increase in metal–oxygen bond dissociation enthalpy for group IV transition metals and oxygen.[53]

As microparticle recoveries improved but remained suboptimal, we implemented digestion method III, increasing the target temperature to 250 °C and maintaining it for 30 minutes before cooling down. This adjustment tremendously increased microparticle recovery rates; nanoparticle recovery remained between 90 and 100%, with a slight improvement observed for nano $ZrO_2$. Additionally, recovery rates for micro rutile $TiO_2$ and micro $ZrO_2$ exceeded 90%. Only micro $HfO_2$ showed comparably low recovery rates of just below 80%.

To further improve micro $HfO_2$ digestion, in digestion method IV, we omitted additional water in the digestion matrix, resulting in a more aggressive acid piranha solution (1.5 mL 97% $H_2SO_4$ + 1 mL 30% $H_2O_2$) and increased peroxomonosulfuric acid (Caro's Acid) formation. Handling this solution generally requires special caution.[38] However, in this setting, we never observed excessive heat or gas development, so we consider working to be sufficiently safe. Under these final conditions, all micro- and nanoparticle recovery rates were found to be well above 90%.

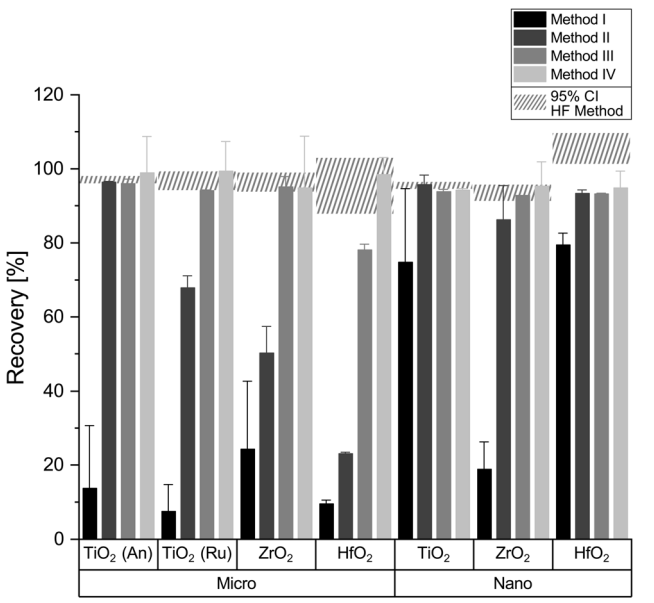


Fig. 1 Metal oxide recoveries for micro- and nanopowders and four different digestion methods determined from measuring the single elements (Ti, Zr, Hf) and calculated using eqn (1); method I: standard $HNO_3$, 10 min@200 °C, method II: $H_2SO_4$, 10 min@200 °C; method III: $H_2SO_4$, 30 min@250 °C, method 4: piranha, 30 min@250 °C; An: anatase, Ru: rutile. Error bars signify $2s_{rel}$ (~95% confidence interval (CI)) and the hatched area the 95% CI of the HF reference method for direct comparison.

### Application of the optimized method for nanoparticle cell uptake quantification

In nanomedical applications, quantifying nanomaterial uptake into cells is crucial for understanding nanomaterial–cell interactions. To demonstrate the applicability of the optimized HF-free digestion method for cell uptake studies, we used digestion method IV to digest nanoparticles spiked to cancer cells (Fig. 2) and investigated the stability of the digested samples over four weeks. Cells were spiked with nanoparticle concentrations up to 10 wt%, representing the higher end of reported cell uptake.[39] All nanoparticles showed recoveries between 80% and 100% with a tendency of higher recoveries for $TiO_2$, followed by $ZrO_2$ and $HfO_2$. All samples remained stable over the course of 4 weeks, indicating that the metals remained stable within the liquid phase, allowing for (re-)evaluation within at least one month.

 This journal is © The Royal Society of Chemistry 2025

Open Access Article. Published on 03 June 2025. Downloaded on 5/18/2026 3:39:33 AM.
This article is licensed under a Creative Commons Attribution 3.0 Unported Licence.

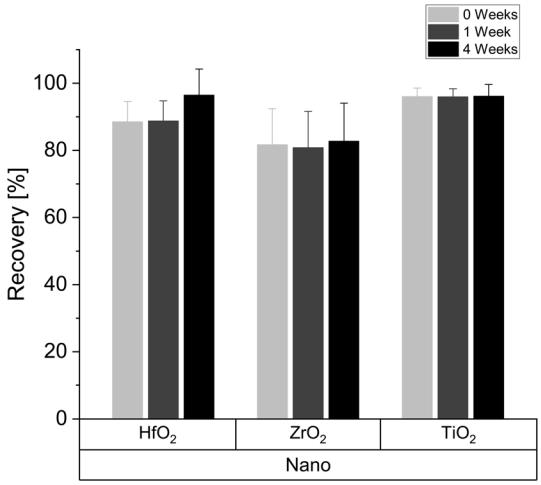


Fig. 2 Metal oxide recoveries for nanopowders spiked to cancer cells quantified directly after digestion (0 weeks) using digestion method IV as well as one and four weeks after digestion. Recoveries were determined from single element (Ti, Zr, Hf) quantifications and calculations using eqn (1). Corresponding nanomaterials were spiked to 100.000 cells per sample resembling a nanomaterial cell-uptake scenario between 1 and 10 wt%. Error bars signify $2s_{rel}$ (~95% confidence interval).

### Application and further method optimization in spiked bovine liver tissue

For *in vivo* toxicity or efficacy studies, metal recovery in organs or target tissues from inserted or injected engineered nano- and micron-sized materials is essential. To simulate such scenarios, the optimized digestion method (IV) was applied to bovine liver tissue (BCR185r) samples spiked with nano- and micro-metal oxide powders.

Metal recoveries were excellent for micro- and nano-$TiO_2$ as well as for all nanopowders (>90%, Fig. 3a). However, the material-dependent decrease in recovery observed during the initial method optimization reappeared (*e.g.*, micro: $TiO_2$ (~100%) > $ZrO_2$ (~85%) > $HfO_2$ (~70%)/nano: $TiO_2$ (~100%) = $ZrO_2$ (~100%) > $HfO_2$ (~90%). Extending the reaction time from 30 to 60 minutes increased metal recoveries to >90% for $ZrO_2$ and $HfO_2$ micropowders as well as $HfO_2$ nanoparticles in liver tissue. Thus, more complex sample matrices require longer reaction times. Furthermore, these results suggest that the method might be also applicable to other types of aqueous and/or organic matter containing samples, such as for example wastewater or sewage sludge. Overall, HF-free digestion method IV provided excellent group IV metal recoveries also in *in vivo* scenarios for both nano- and microparticles. Additionally, digested samples displayed a very good long term sample stability post digestion of at least four weeks (Fig. 3b).

Table 2 Detection limit (DL), quantification limit (QL) and calibration slope (sensitivity) for each element (Ti, Zr, Hf) for the HF-free and the HF reference digestion method as quantified using ICP-OES

| | | HF-free method | | HF method | |
|---|---|---|---|---|---|
| Limits of detection | | Method (ppb) | Instrument (ppb) | Method (ppb) | Instrument (ppb) |
| Ti | DL | 0.69 | 0.21 | 0.37 | 0.34 |
| | LOQ | 2.10 | 0.63 | 1.12 | 1.03 |
| | Slope | 96.16 Int. $ppb^{-1}$ | | 96.03 Int. $ppb^{-1}$ | |
| Zr | DL | 2.23 | 0.71 | 0.86 | 1.03 |
| | LOQ | 6.76 | 2.14 | 2.62 | 3.13 |
| | Slope | 88.08 Int. $ppb^{-1}$ | | 89.05 Int. $ppb^{-1}$ | |
| Hf | DL | 10.52 | 1.90 | 1.95 | 1.69 |
| | QL | 31.87 | 5.76 | 5.89 | 5.13 |
| | Slope | 5.27 Int. $ppb^{-1}$ | | 5.35 Int. $ppb^{-1}$ | |

## Sensitivity and detection limits of HF-free *vs.* HF digestion method

Finally, ICP-OES detection limits and sensitivity were compared between the HF-free and HF reference digestion method. The

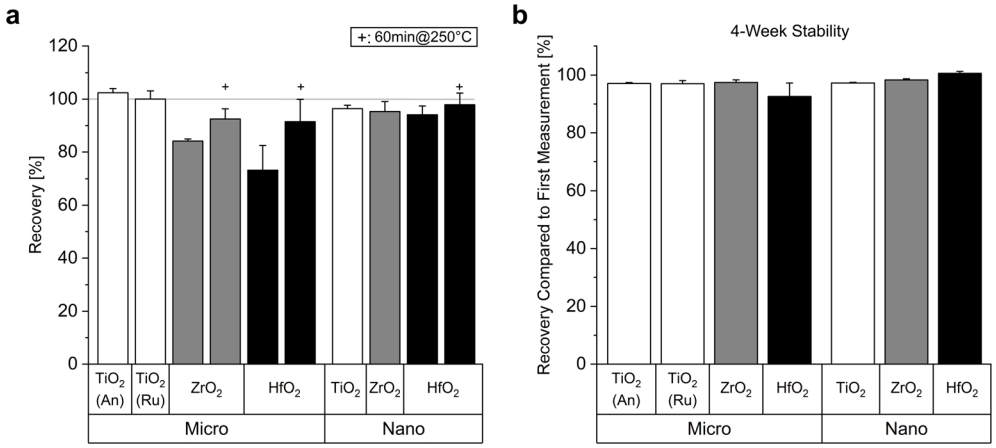


Fig. 3 (a) Metal oxide recoveries for micro- and nanopowders mixed with bovine liver tissue simulating an *in vivo* scenario after digestion using method IV or an adapted method IV with a longer microwave reaction time at 250 °C (60 instead of 30 minutes, indicated by the "+" sign). Recoveries were determined from single element (Ti, Zr, Hf) quantifications and calculations using eqn (1). (b) Four-weeks stability of digested samples plotted as recovery compared to the first measurement in (a) performed directly after digestion; An: anatase, Ru: rutile. Error bars signify $2s_{rel}$ (~95% confidence interval).

Open Access Article. Published on 03 June 2025. Downloaded on 5/18/2026 3:39:33 AM. This article is licensed under a Creative Commons Attribution 3.0 Unported Licence.

detection and quantification limits (DL and QL, respectively) were calculated per FDA guidelines: $DL = \frac{3.3\sigma}{slope}$ and $QL = \frac{10\sigma}{slope}$, where $\sigma$ is the standard deviation of the blank response (here: emission intensity).[43] Sensitivities, indicated by calibration slopes (intensity/ppb), were comparable for both methods, following atomic number order (Ti: ~96 Int. $ppb^{-1}$ > Zr: ~88 Int. $ppb^{-1}$ > Hf: ~5 Int $ppb^{-1}$, Table 2). Consequently, detection and quantification limits followed this trend but were generally slightly lower for the HF method. While the instrument and method DLs and QLs of the HF method were very similar to each other, they showed a discrepancy to those of the HF-free method. This is because the standard deviation of the procedure blanks was generally higher for the HF-free method compared to the HF method. This behavior might be attributed to matrix differences (2.9% $H_2SO_4$ compared to 2% $HNO_3$) which can affect viscosity and, consequently, nebulization and transport efficacies in both methods. This is supported by the observation that the DL and QL can be lowered by roughly a factor 2–3 by doubling the readout time (ESI, Table S8†). Further improvements in DLs and QLs can be achieved by implementing tube pre-cleaning procedures to prevent analyte carryover between measurement campaigns and by increasing rinsing time between individual measurements. Nevertheless, given the comparable quantification sensitivities and the similar ranges of detection and quantification limits, we conclude that the HF-free method is a viable alternative to the reference HF digestion method which can be used in every standardly equipped analytical laboratory.

## Conclusion

The reliable detection of group IV metal oxides is playing an increasingly important role in the biomedical as well as environmental fields. To digest group IV metal oxide materials, HF- or fusion-based methods are standardly used to date. Here, we have shown that sulfuric acid and hydrogen peroxide can be used as easily available, comparatively safe alternative HF-free digestion method for Ti, Zr and Hf metal oxides, both as pure powders and in aqueous environments with organic matter (cells, tissues). While nanomaterials were easier to digest, micron-sized powders required higher reaction temperatures, longer reaction times, and higher concentrations of peroxomonosulfuric acid for successful digestion. Digestion efficacy was also atomic number dependent. The proposed methods can be used to quantify the oxide elements in cells, organs and tissues from average particle sizes <6 nm up to 860 nm. ICP-OES revealed good linearity between 0.01 and 5 mg $L^{-1}$ (corresponding to 0.005–2.5 ng $cell^{-1}$, considering 100 000 digested cells per sample, or, 0.25–12.5 mg $g^{-1}$ of dried tissue, considering 20 mg digested tissue per sample) and common metal-dependent detection limits, comparable to those of an HF-containing reference method. The proposed HF-free method has fewer safety and infrastructural demands compared to HF digestions and allows cheaper and easier access to pre-clinical and clinical toxicity as well as efficacy studies with group IV metal oxide materials.

## Data availability

The data supporting this article have been included as part of the ESI.†

## Author contributions

LRHG: investigation, methodology, validation, formal analysis, data curation, writing – original draft, writing – review & editing; MR: formal analysis, writing – review & editing; IKH: resources, funding acquisition, writing – review & editing; AG: conceptualization, supervision, validation, writing – original draft, writing – review & editing.

## Conflicts of interest

There are no conflicts to declare.

## Acknowledgements

This work received funding from EU Project MetrINo (Project number 22HLT04) and the Ria & Arthur Dietschweiler foundation. Andreas Voegelin and Ralf Kaegi (EAWAG) are kindly acknowledged for granting us access to their HF lab as well as Brian Sinnet and Matthias Philipp for on-site support.

## References

1 H.-L. Tu, H.-B. Zhao, Y.-Y. Fan and Q.-Z. Zhang, Recent developments in nonferrous metals and related materials for biomedical applications in china: a review, *Rare Met.*, 2022, **41**(5), 1410–1433, DOI: **10.1007/s12598-021-01905-y**.

2 L. R. H. Gerken, A. L. Neuer, P. M. Gschwend, K. Keevend, A. Gogos, A. H. C. Anthis, L. Aengenheister, S. E. Pratsinis, L. Plasswilm and I. K. Herrmann, Scalable synthesis of ultrasmall metal oxide radio-enhancers outperforming gold, *Chem. Mater.*, 2021, **33**(9), 3098–3112, DOI: **10.1021/acs.chemmater.0c04565**.

3 L. R. H. Gerken, A. Gogos, F. H. L. Starsich, H. David, M. E. Gerdes, H. Schiefer, S. Psoroulas, D. Meer, L. Plasswilm, D. C. Weber and I. K. Herrmann, Catalytic activity imperative for nanoparticle dose enhancement in photon and proton therapy, *Nat. Commun.*, 2022, **13**(1), 3248, DOI: **10.1038/s41467-022-30982-5**.

4 J. Wang, J. Pan, Y. Tang, J. Chen, X. Fei, W. Xue and X. Liu, Advances of hafnium based nanomaterials for cancer theranostics, *Front. Chem.*, 2023, **11**, 1283924, DOI: **10.3389/fchem.2023.1283924**.

5 F. U. Rehman, C. Zhao, H. Jiang and X. Wang, Biomedical applications of nano-titania in theranostics and photodynamic therapy, *Biomater. Sci.*, 2015, **4**(1), 40–54, DOI: **10.1039/C5BM00332F**.

6 A. M. Bannunah, Biomedical applications of zirconia-based nanomaterials: challenges and future perspectives, *Molecules*, 2023, **28**(14), 5428, DOI: **10.3390/molecules28145428**.

 This journal is © The Royal Society of Chemistry 2025

Open Access Article. Published on 03 June 2025. Downloaded on 5/18/2026 3:39:33 AM. This article is licensed under a Creative Commons Attribution 3.0 Unported Licence.

7 J. Wang, Z. Wang, W. Wang, Y. Wang, X. Hu, J. Liu, X. Gong, W. Miao, L. Ding, X. Li and J. Tang, Synthesis, modification and application of titanium dioxide nanoparticles: a review, *Nanoscale*, 2022, **14**(18), 6709–6734, DOI: 10.1039/D1NR08349J.

8 A. K. Chitoria, A. Mir and M. A. Shah, A review of $ZrO_2$ nanoparticles applications and recent advancements, *Ceram. Int.*, 2023, **49**(20), 32343–32358, DOI: 10.1016/j.ceramint.2023.06.296.

9 M. Kumar, S. Halder and A. Kumar, A review of biomedical applications of zirconia-based nanomaterials, in *Advances in Materials Engineering*, ed. P. Bhingole, K. Joshi, S. D. Yadav and A. Sharma, Springer Nature, Singapore, 2025, pp. 71–81, DOI: 10.1007/978-981-97-7114-1_7.

10 S. Ayyaru, V. Jayaraman and Y.-H. Ahn, Non-precious $HfO_2$ nanoparticle as an alternative cathode catalyst for microbial fuel cell applications, *Int. J. Hydrogen Energy*, 2024, **57**, 679–687, DOI: 10.1016/j.ijhydene.2024.01.043.

11 A. Pandey and S. Sahoo, Progress on medical implant: a review and prospects, *J. Bionic Eng.*, 2023, **20**(2), 470–494, DOI: 10.1007/s42235-022-00284-z.

12 J. Grech and E. Antunes, Zirconia in dental prosthetics: a literature review, *J. Mater. Res. Technol.*, 2019, **8**(5), 4956–4964, DOI: 10.1016/j.jmrt.2019.06.043.

13 G. E. Romanos, G. A. Fischer and R. Delgado-Ruiz, Titanium wear of dental implants from placement, under loading and maintenance protocols, *Int. J. Mol. Sci.*, 2021, **22**(3), 1067, DOI: 10.3390/ijms22031067.

14 D. Chappard, L. Rony, F. Ducellier, V. Steiger and L. Hubert, Wear debris released by hip prosthesis analysed by microcomputed tomography, *J. Microsc.*, 2021, **282**(1), 13–20, DOI: 10.1111/jmi.12971.

15 A. Stricker, T. Bergfeldt, T. Fretwurst, O. Addison, R. Schmelzeisen, R. Rothweiler, K. Nelson and C. Gross, Impurities in commercial titanium dental implants – A mass and optical emission spectrometry elemental analysis, *Dent. Mater.*, 2022, **38**(8), 1395–1403, DOI: 10.1016/j.dental.2022.06.028.

16 L. R. H. Gerken, M. E. Gerdes, M. Pruschy and I. K. Herrmann, Prospects of nanoparticle-based radioenhancement for radiotherapy, *Mater. Horiz.*, 2023, **10**(10), 4059–4082, DOI: 10.1039/D3MH00265A.

17 S. Sargazi, S. Er, S. Sacide Gelen, A. Rahdar, M. Bilal, R. Arshad, N. Ajalli, M. Farhan Ali Khan and S. Pandey, Application of titanium dioxide nanoparticles in photothermal and photodynamic therapy of cancer: an updated and comprehensive review, *J. Drug Deliv. Sci. Technol.*, 2022, **75**, 103605, DOI: 10.1016/j.jddst.2022.103605.

18 L. R. H. Gerken, C. Beckers, B. A. Brugger, V. M. Kissling, A. Gogos, S. Wee, M. R. Lukatskaya, H. Schiefer, L. Plasswilm, M. Pruschy and I. K. Herrmann, Catalytically active Ti-based nanomaterials for hydroxyl radical mediated clinical X-ray enhancement, *Adv. Sci.*, 2024, **11**(47), 2406198, DOI: 10.1002/advs.202406198.

19 M. J. Neufeld, A. Lutzke, G. Pratx and C. Sun, High-Z metal–organic frameworks for X-ray radiation-based cancer theranostics, *Chemistry*, 2021, **27**(10), 3229–3237, DOI: 10.1002/chem.202003523.

20 A. L. Neuer, A. Jessernig, L. R. H. Gerken, A. Gogos, F. H. L. Starsich, A. H. C. Anthis and I. K. Herrmann, Cellular fate and performance of group IV metal organic framework radioenhancers, *Biomater. Sci.*, 2022, **10**(22), 6558–6569, DOI: 10.1039/D2BM00973K.

21 C. Le Tourneau, C. Hoffmann, Z. Takacsi-Nagy, X. Liem, S. Salas, A. Debard, L. Finzi, L. A. Farber, M. Gogishvili, G. Kristesashvili, T. Makharadze and S. S. Yom, NANORAY-312: a phase III pivotal study of NBTXR3 activated by investigator's choice of radiotherapy alone or radiotherapy in combination with cetuximab for platinum-based chemotherapy-ineligible elderly patients with locally advanced head and neck squamous cell carcinoma, *J. Clin. Oncol.*, 2022, **40**(16_suppl), TPS6110, DOI: 10.1200/JCO.2022.40.16_suppl.TPS6110.

22 M. Spiotto, L. E. Feldman, J. J. Luke, G. F. Fleming, D. Olson, J. W. Moroney, R. Nanda, A. Rosenberg, A. T. Pearson, A. Juloori, F. Weinberg, C. Ray, R. C. Gaba, P. J. Chang, L. A. Janisch, Z.-Q. Xu, W. Lin, R. R. Weichselbaum and S. J. Chmura, A phase 1 dose-escalation study of RiMO-301 with palliative radiation in advanced tumors, *J. Clin. Oncol.*, 2023, **41**(16_suppl), 2527, DOI: 10.1200/JCO.2023.41.16_suppl.2527.

23 S. Bonvalot, P. L. Rutkowski, J. Thariat, S. Carrère, A. Ducassou, M.-P. Sunyach, P. Agoston, A. Hong, A. Mervoyer, M. Rastrelli, V. Moreno, R. K. Li, B. Tiangco, A. C. Herraez, A. Gronchi, L. Mangel, T. Sy-Ortin, P. Hohenberger, T. de Baère, A. Le Cesne, S. Helfre, E. Saada-Bouzid, A. Borkowska, R. Anghel, A. Co, M. Gebhart, G. Kantor, A. Montero, H. H. Loong, R. Vergés, L. Lapeire, S. Dema, G. Kacso, L. Austen, L. Moureau-Zabotto, V. Servois, E. Wardelmann, P. Terrier, A. J. Lazar, J. V. M. G. Bovée, C. Le Péchoux and Z. Papai, NBTXR3, a first-in-class radioenhancer hafnium oxide nanoparticle, plus radiotherapy *versus* radiotherapy alone in patients with locally advanced soft-tissue sarcoma (Act.In.Sarc): a multicentre, phase 2–3, randomised, controlled trial, *Lancet Oncol.*, 2019, **20**(8), 1148–1159, DOI: 10.1016/S1470-2045(19)30326-2.

24 S. Grosse, H. K. Haugland, P. Lilleng, P. Ellison, G. Hallan and P. J. Høl, Wear particles and ions from cemented and uncemented titanium-based hip prostheses—A histological and chemical analysis of retrieval material, *J. Biomed. Mater. Res., Part B*, 2015, **103**(3), 709–717, DOI: 10.1002/jbm.b.33243.

25 S. Shah, S. Nene, N. Rangaraj, R. S. Raghuvanshi, S. B. Singh and S. Srivastava, Bridging the gap: academia, industry and FDA convergence for nanomaterials, *Drug Dev. Ind. Pharm.*, 2020, **46**(11), 1735–1746, DOI: 10.1080/03639045.2020.1821055.

26 Y. Li, Y. Qi, H. Zhang, Z. Xia, T. Xie, W. Li, D. Zhong, H. Zhu and M. Zhou, Gram-scale synthesis of highly biocompatible and intravenous injectable hafnium oxide nanocrystal with enhanced radiotherapy efficacy for cancer theranostic, *Biomaterials*, 2020, **226**, 119538, DOI: 10.1016/j.biomaterials.2019.119538.

Open Access Article. Published on 03 June 2025. Downloaded on 5/18/2026 3:39:33 AM. This article is licensed under a Creative Commons Attribution 3.0 Unported Licence.

27 N. Yu, W. Tu, P. Qiu, Q. Ren, X. Chen, M. Zhu, Y. Liu and Z. Chen, Full-route advances *via* biomimetic and biodegradable ultrasmall-in-nano architectures with radiation-photo synergy, *Nano Today*, 2022, **43**, 101427, DOI: 10.1016/j.nantod.2022.101427.

28 T. L. McGinnity, O. Dominguez, T. E. Curtis, P. D. Nallathamby, A. J. Hoffman and R. K. Roeder, Hafnia ($HfO_2$) nanoparticles as an X-ray contrast agent and mid-infrared biosensor, *Nanoscale*, 2016, **8**(28), 13627–13637, DOI: 10.1039/C6NR03217F.

29 A. F. Holleman, *Lehrbuch Der Anorganischen Chemie*, Walter de Gruyter GmbH & Co KG, 102nd edn, 2007, p. 1527.

30 M. Mutsuga, K. Sato, Y. Hirahara and Y. Kawamura, Analytical methods for $SiO_2$ and other inorganic oxides in titanium dioxide or certain silicates for food additive specifications, *Food Addit. Contam., :Part A*, 2011, **28**(4), 423–427, DOI: 10.1080/19440049.2010.551548.

31 A. Salvador, M. C. Pascual-Martí, J. R. Adell, A. Requeni and J. G. March, Analytical methodologies for atomic spectrometric determination of metallic oxides in UV sunscreen creams, *J. Pharm. Biomed. Anal.*, 2000, **22**(2), 301–306, DOI: 10.1016/S0731-7085(99)00286-1.

32 K. Khosravi, M. E. Hoque, B. Dimock, H. Hintelmann and C. D. Metcalfe, A novel approach for determining total titanium from titanium dioxide nanoparticles suspended in water and biosolids by digestion with ammonium persulfate, *Anal. Chim. Acta*, 2012, **713**, 86–91, DOI: 10.1016/j.aca.2011.11.048.

33 N. Kim, C. Kim, S. Jung, Y. Park, Y. Lee, J. Jo, M. Hong, S. Lee, Y. Oh and K. Jung, Determination and identification of titanium dioxide nanoparticles in confectionery foods, marketed in south korea, using inductively coupled plasma optical emission spectrometry and transmission electron microscopy, *Food Addit. Contam. Part A*, 2018, **35**(7), 1238–1246, DOI: 10.1080/19440049.2018.1482011.

34 A. F. Holleman, *Lehrbuch Der Anorganischen Chemie*, Walter de Gruyter GmbH & Co KG, 102nd edn, 2007, p. 1539.

35 Y. Ma, S. Stopic, L. Gronen and B. Friedrich, Recovery of Zr, Hf, Nb from eudialyte residue by sulfuric acid dry digestion and water leaching with $H_2O_2$ as a promoter, *Hydrometallurgy*, 2018, **181**, 206–214, DOI: 10.1016/j.hydromet.2018.10.002.

36 P. S. Watkins, B. T. Castellon, C. Tseng, M. V. Wright, C. W. Matson and G. P. Cobb, Validation of a sulfuric acid digestion method for inductively coupled plasma mass spectrometry quantification of $TiO_2$ nanoparticles, *Bull. Environ. Contam. Toxicol.*, 2018, **100**(6), 809–814, DOI: 10.1007/s00128-018-2336-2.

37 A. L. Neuer, D. Geck, A. Gogos, V. M. Kissling, A. Balfourier and I. K. Herrmann, Nanoanalytical insights into the stability, intracellular fate, and biotransformation of metal–organic frameworks, *ACS Appl. Mater. Interfaces*, 2023, **15**(32), 38367–38380, DOI: 10.1021/acsami.3c08818.

38 H. G. Schmidt, Safe piranhas: a review of methods and protocols, *ACS Chem. Health Saf.*, 2022, **29**(1), 54–61, DOI: 10.1021/acs.chas.1c00094.

39 B. Rudek, A. McNamara, J. Ramos-Méndez, H. Byrne, Z. Kuncic and J. Schuemann, Radio-enhancement by gold nanoparticles and their impact on water radiolysis for X-ray, proton and carbon-ion beams, *Phys. Med. Biol.*, 2019, **64**(17), 175005, DOI: 10.1088/1361-6560/ab314c.

40 X. Liem, T. de Baère, O. I. Vivar, T. Y. Seiwert, C. Shen, Z. Pápai, V. Moreno, Z. Takácsi-Nagy, F. Helfferich, J. Thariat, Z. Gooi, S. S. Yom, P. Bossi, R. L. Ferris, T. G. Hackman, C. Le Tourneau, J. Rodriguez and C. Hoffmann, International guidelines for intratumoral and intranodal injection of NBTXR3 nanoparticles in head and neck cancers, *Head Neck*, 2024, **46**(6), 1253–1262, DOI: 10.1002/hed.27739.

41 S. Kromidas, *Validierung in der Analytik*, Wiley-VCH, Weinheim, 2012.

42 N. Doebelin and R. Kleeberg, Profex: a graphical user interface for the rietveld refinement program BGMN, *J. Appl. Crystallogr.*, 2015, **48**(5), 1573–1580, DOI: 10.1107/S1600576715014685.

43 FDA, *Q2(R2) Validation of Analytical Procedures*, https://www.fda.gov/regulatory-information/search-fda-guidance-documents/q2r2-validation-analytical-procedures, accessed 2025 April 24.

44 H. He, F. Xu, Q. Li, P. Dong, J. Zheng, C. Wu, Z. He, J. Qu, Z. Xu, R. Chi and M. Wu, Separation of hafnium from zirconium in $HNO_3$ solution by solvent extraction with Cyanex572, *Hydrometallurgy*, 2021, **202**, 105600, DOI: 10.1016/j.hydromet.2021.105600.

45 L. Y. Wang and M. S. Lee, A review on the aqueous chemistry of Zr(IV) and Hf(IV) and their separation by solvent extraction, *J. Ind. Eng. Chem.*, 2016, **39**, 1–9, DOI: 10.1016/j.jiec.2016.06.004.

46 $HfO_2$ Monoclinic – MP ID: Mp-352, https://next-gen.materialsproject.org/materials/mp-352.

47 $ZrO_2$ Monoclinic – MP ID: Mp-2858, https://next-gen.materialsproject.org/materials/mp-2858.

48 $TiO_2$ Anatase – MP ID: Mp-390, https://next-gen.materialsproject.org/materials/mp-390.

49 $TiO_2$ Rutile – MP ID: Mp-2657, https://next-gen.materialsproject.org/materials/mp-2657.

50 $HfO_2$ Orthorhombic – MP ID: Mp-1858, https://next-gen.materialsproject.org/materials/mp-1858.

51 Z. Wang, Z. Ni, D. Qiu, G. Tao and P. Yang, Determination of impurities in titanium nitride by slurry introduction axial viewed inductively coupled plasma optical emission spectrometry, *Spectrochim. Acta, Part B*, 2005, **60**(3), 361–367, DOI: 10.1016/j.sab.2004.12.006.

52 L. Ebdon, M. Foulkes and K. Sutton, Slurry nebulization in plasmas, *J. Anal. At. Spectrom.*, 1997, **12**(2), 213–229, DOI: 10.1039/A604914A.

53 K. A. Moltved and K. P. Kepp, The chemical bond between transition metals and oxygen: electronegativity, d-orbital effects, and oxophilicity as descriptors of metal–oxygen interactions, *J. Phys. Chem. C*, 2019, **123**(30), 18432–18444, DOI: 10.1021/acs.jpcc.9b04317.

 This journal is © The Royal Society of Chemistry 2025